High Dynamic Range AFM Cantilever With a Collocated Piezoelectric Actuator-Sensor Pair

Mohammad Mahdavi, M. Bulut Coskun, and S. O. Reza Moheimani, *Fellow, IEEE*

***Abstract*— We present a novel approach to fundamentally eliminate electrical feedthrough (cross-talk) signal in self-sensing piezoelectric microcantilevers, used in dynamic mode atomic force microscopy (AFM). The probe is an Si microcantilever on which a two-layer piezoelectric stack transducer is microfabricated. The top transducer in the stack functions as an actuator, while the bottom transducer is used as a deflection sensor. This arrangement leads to a collocated actuator-sensor pair that coexist on the same surface area. We report experimental results that establish the sensor's ability to capture the full dynamic range of the cantilever with minimal feedthrough from the actuator. [2019-0143]**

***Index Terms*— Atomic force microscopy (AFM), tapping mode AFM, active microcantilever, piezoelectric self-sensing, on-chip feedthrough cancellation, dynamic range, microelectromechanical system (MEMS).**

I. Introduction

AMPLITUDE-MODULATED atomic force microscopy (AFM), also known as the tapping-mode AFM, is widely used for capturing surface topographies and analyzing material properties at the nanoscale [1]. This method relies on changes in vibration amplitude of an AFM probe, while it is being scanned over a surface. The probe is a microcantilever driven to vibrate at its first flexural resonance mode and brought in close proximity to the surface. While the vibrating cantilever scans over the surface, a sharp tip located at the free end of the cantilever makes intermittent contact with the surface. Interfacial forces between the cantilever's tip and the sample modulate vibration amplitude of the cantilever. A deflection sensor translates vibrations of the cantilever to an electronic signal, which is then fed to an amplitude demodulator that extracts envelope of the high-frequency signal. A PI controller drives a z-actuator that adjusts the vertical position of the cantilever, relative to the sample, in order to keep the vibration amplitude constant. The control effort is then plotted to construct the surface topography.

Manuscript received June 22, 2019; revised December 21, 2019; accepted January 14, 2020. Date of publication February 4, 2020; date of current version April 2, 2020. Subject Editor L. Buchaillot. This work was supported by the U.S. Department of Energy's Office of Energy Efficiency and Renewable Energy (EERE) under the Advanced Manufacturing Office Award Number DEEE0008322. *(Corresponding author: S. O. Reza Moheimani.)*

Mohammad Mahdavi and S. O. Reza Moheimani are with the Department of Systems Engineering, The University of Texas at Dallas, Richardson, TX 75080 USA (e-mail: reza.moheimani@utdallas.edu).

M. Bulut Coskun was with the Department of Systems Engineering, The University of Texas at Dallas, Richardson, TX 75080 USA. He is now with the Advanced Optical and Electromechanical Microsystems Group, Jet Propulsion Laboratory, Pasadena, CA 91109 USA.

Color versions of one or more of the figures in this article are available online at http://ieeexplore.ieee.org.

Digital Object Identifier 10.1109/JMEMS.2020.2967794

Optical beam deflection (OBD) is a well established technique, widely used in commercial AFMs, to measure the cantilever deflection [2]. In this method, a focused laser beam is reflected from the free end of the cantilever and captured by a position sensitive photodetector (PSPD) that maps cantilever's deflections to a signal. This is an efficient approach to cantilever deflection measurement, which enables the AFM to achieve atomic resolution. However, since the sensor is not integrated with the cantilever, it requires frequent adjustments. Furthermore, using a single optical sensor to measure deflection of an array of cantilevers is not a straightforward task. In a conventional setup, the microcantilever is mounted on a piezoelectric actuator that oscillates the microcantilever. Due to the large size of this actuator, relative to the dimensions of the cantilever, unintended frequencies, in addition to the resonance frequency of the cantilever, are generated. This, in turn, makes controlling the dynamics of the cantilever challenging. Therefore, a microcantilever with embedded actuation and sensing capabilities is highly desirable.

There have been attempts to use MEMS processes in order to realize AFM contilevers with integrated sensors and actuators. In particular, bimorph actuation based on piezoelectric [3] and electrothermal [4] transduction methods have been employed to actuate Si cantilevers. Electrical charge, induced in the piezoelectric transducer, has been used to measure vibration of piezoelectric cantilevers [3], [5]. In electrothermally actuated cantilevers, measurements of a piezoresistor obtained from a Wheatston bridge have been used for sensing [4], [6].

AFM imaging with commercially available piezoelectric microcantilevers has been previously demonstrated [3], [5], [7], [8]. The cantilevers used in these studies contain a layer of ZnO piezoelectric material sandwiched between two metal layers serving as electrodes. The actuation voltage is applied to the top electrode to oscillate the cantilever at its resonance frequency. The electrical charge resulting from the piezoelectric effect is measured using a readout circuit. For an ideal cantilever with a quality factor $Q \gg 1$, the vibration amplitude at resonance is approximately Q times larger than when it is operating off resonance. If the piezoelectric sensor follows the cantilever dynamics well, one should be able to make the same observation with the piezoelectric charge. In practice, however, the piezoelectrically induced charge is significantly less than the electrically induced charge due to dielectric properties of the piezoelectric layer. This is known as the "feedthrough effect" [3], [9], since the charge is induced through an unintended electrical path from the input to the output.

The feedthrough effect has also been a common bottleneck in capturing true dynamics of piezoelectric and capacitive

micro-resonators. In order to restore the dynamic response of the resonators from their output charge, several feedthrough cancellation methods have been proposed [10]–[15]. Similar apporaches have been implemented for feedthrough cancellation in piezoelectric cantilevers [3], [5], [9], [16]–[20]. One approach is based on electronically mimicking the feedthrough path using a capacitance with the same value as the feedthrough capacitance of the piezoelectric layer, and subtracting its charge from the output charge of the cantilever [3]. The resulting dynamic range is satisfactory for many tapping mode AFM applications. However, the method is rather complicated, and its extension to more than one mode may be difficult. An alternative approach is to increase the electrical isolation between input and output electrodes by physically separating the piezoelectric actuator from the sensor [9], [19]. This allows for three possibilities. In a three port configuration, bottom electrodes of both transducers are grounded. The actuation voltage is applied to the top electrode of one transducer and the charge is measured at the top electrode of the other [19]. Alternatively, if three piezoelectric transducers are available, differential sensing may be perfomed. The actuation voltage is applied to the middle transducer with a grounded bottom electrode. The remaining two transducers are grounded at opposite electrodes to enable charge sensing with 180° phase shift, and thus differential sensing. Combining the two signals removes the feedthroughs associated with the two sense paths [9], [16]. Finally, in a pseudo actuation configuration, a parallel path with a tunable gain is established through a separate dielectric layer to reduce the the piezoelectric path's electrical feedthrough [9].

These approaches can minimize the feedthrough to a reasonable extent. However, for most users of the AFM they could be difficult to implement. Furthermore, their efficiency may be limited when applied to high-frequency cantilevers since they require dividing cantilever surface between actuation and sense transducers. Here, we propose a microfabricated two-layer piezoelectric transducer that results in a collocated actuator-sensor pair. Stacking the two piezoelectric transducers enables the most optimal use of limited space available on the cantilever surface. We provide *ab-initio* analysis and finite element simulation that shows how reducing the feedthrough capacitance leads to a significant reduction of the feedthrough effect. We describe a microfabrication process that we developed to realize the proposed device. We characterize a fabricated cantilever and demonstrate that experimental results closely match the simulated behavior of the device. We conclude by reporting AFM images obtained with this cantilever on two calibration gratings.

II. Electromechanical Design

A. Microcantilevers With Collocated Transducers

A MEMS piezoelectric active cantilever consists of a thin Si layer on which a piezoelectric transducer is fabricated in between two electrodes; see Fig. 1(a). Such configuration allows fabrication of a cantilever with collocated transducers. It has been previously shown that collocation of transducers on a microcantilever offers several adavantages in controlling the dynamics of the cantilver in a closed-loop system [17], [21].

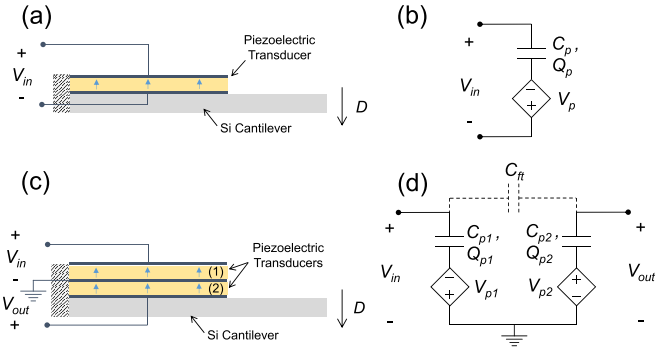

Fig. 1. (a) A microcantilever with a single piezoelectric transducer, (b) a simple electrical model of the piezoelectric cantilever, (c) a cantilever with a two-layer piezoelectric transducer, and (d) an electrical model for the two-layer piezoelectric cantilever.

Upon application of a voltage, the piezoelectric transducer mechanically strains, and this in turn results in out-of-plane deflection of the cantilever. Therefore, the first modal response at the free end of the cantilever, due to the applied voltage V_{in}, can be expressed as [3]:

$$D(s) = \frac{\alpha\omega_0^2}{s^2 + \frac{\omega_0}{Q}s + \omega_0^2} V_{in}(s), \tag{1}$$

where ω_0 is the first resonance frequency of the cantilever, α is an electromechanical coupling factor and Q is the quality factor of the first mode. When the transducer is mechanically strained, due to the piezoelectric effect, electric charges appear on the transducer's electrodes. This can be modeled by a strain dependent voltage source V_p in series with a capacitance C_p, representing the dielectric effect of the piezoelectric layer (see Fig. 1(b)) [21]. The relationship between the electric charge Q_p and the applied voltage V_{in} can be stated as [3]:

$$Q_p(s) = \frac{\beta\omega_0^2}{s^2 + \frac{\omega_0}{Q}s + \omega_0^2} V_{in}(s) + C_p V_{in}(s), \tag{2}$$

where β is an electromechanical coupling factor associated with the piezoelectric effect. Based on Eq. 2, the total charge on the sense electrode is a combination of an electromechanically induced charge due to the piezoelectric effect and an electrically induced charge through the dielectric capacitance of the piezoelectric layer. While the first term follows the cantilever's dynamics, the second term is an undesired effect which is often referred to as the feedthrough. In a MEMS piezoelectric cantilever, the second term is dominant which conceals the desired cantilever dynamics. To recover the dynamic response of the cantilever measured with the piezoelectric deflection sensor, the second term must be eliminated or significantly reduced.

In the previous section we discussed various techniques that have been employed to minimize the feedthrough either electronically or at the device level. An effective approach to reduce the feedthrough is based on physically separating the sensing and actuation functionalities into two separate transducers. If sensor and actuator are both microfabricated from the same piezoelectric layer, the designer would need to strike a compromise between the space allocated to each

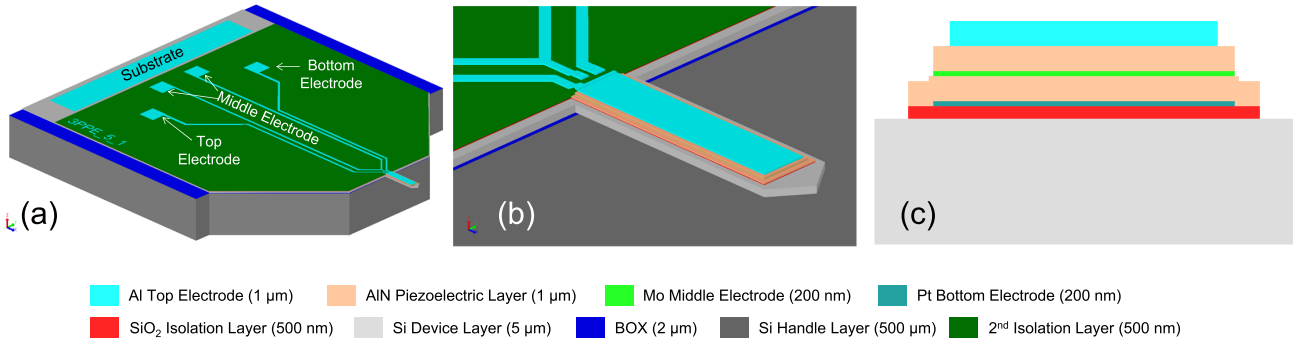

Fig. 2. (a) The structure of two-layer piezoelectric cantilever with its electrical connections, (b) zoomed-in view of the cantilever, and (c) cross-sectional view of the cantilever and its constructive materials.

transducer and their respective efficiencies. This is due to the fact that a piezoelectric sensor's electromechanical coupling factor is a function of its electrode surface area [21]. Therefore, a large sensor size is highly desirable. However, one would need to allocate adequate space to the actuator to ensure its efficient functionality. This issue can be resolved by stacking the sensor and actuator on the cantilever. This is illustrated in Fig. 1(c), where a two-layer piezoelectric actuator-sensor pair is microfabricated on a Si cantilever with three different terminations at the top, middle and bottom electrodes.

The two-layer transducer can be modeled by doubling the model of a single transducer cantilever as illustrated in Fig. 1(d). The path from the input is bypassed to the ground, therefore the dielectric capacitance does not directly contribute to the output charge. Ideally, in this configuration, the feedthrough effect is completely eliminated, and the charge measured on the sense electrode has a strong correlation with the cantilever dynamics. We will show later through finite element analysis that a small stray capacitance C_{ft} will result in a feedthrough. However, this capacitance is by far smaller than transducer's dielectric capacitance, and can thus be neglected in comparison with the dynamical response of the cantilever.

B. The Proposed Structure

The two layer piezoelectric cantilevers are built on a silicon-on-insulator (SOI) substrate, which consists of a 5 μm thick device layer (DL), a 2 μm thick SiO_2 buried oxide (BOX) layer and 500 μm thick handle layer. The cantilevers, made out of the device layer, are 350 μm in length and 100 μm in width. In order to stimulate the cantilever into vibrations and measure its deflections, a stack of two-layer piezoelectric transducers is microfabricated on the Si cantilever. The stack is made of a 200 nm thick Pt, a bottom 1 μm thick AlN piezoelectric layer, a 200 nm thick Mo layer, a top 1 μm thick AlN piezoelectric layer and 1 μm thick Al layer, which are served respectively as the bottom electrode layer, the bottom piezoelectric transducer, the middle electrode layer, the top piezoelectric transducer and the top electrode layer from bottom to top. The complete structure of the device, as well as a close-up view of the cantilever are shown in Fig. 2(a-b). Fig. 2(c) shows a cross-sectional view of the cantilever with its constructing materials.

Aluminum wirebond pads provide electrical connections to the three electrodes of the cantilever, labeled in Fig. 2(a). A wide Al pad provides electrical connection to the Si device layer. Grounding the substrate is necessary to avoid further stray capacitances through the substrate. The SiO_2 layer under the stacked layers provides electrical isolation between the bottom electrode and the Si substrate. The middle electrode is connected to the ground, the top electrode is connected to the actuation voltage, and the bottom electrode is used as readout of the piezoelectric strain signal which serves as a measure of cantilever deflection. The actuation voltage across the top piezoelectric layer produces a stress along the length of the cantilever, consequently causing the cantilever to deflect. Meanwhile, cantilever vibrations produce electric charges which are accumulated on the bottom electrode. The two-layer transducer enables three port operation of the cantilever to minimize the feedthrough level.

C. Finite Element Simulation

Prior to microfabrication, finite element simulations are conducted to evaluate performance of the proposed cantilever using CoventorWare software package. Using the Fast Frequency Response Simulation (Fast PZE) module, wideband frequency responses of the cantilever between 60 kHz and 100 kHz are obtained. The first flexural mechanical resonance mode of the cantilever exists in this frequency range. For this reason, the 3D model, illustrated in Fig. 2(a), is constructed and simulated in the finite element analysis (FEA) software package. In this simulation, the basic relationship between charge and voltage in piezoelectric physics model is used to extract an electromechanical model of the structure and electrical capacitors between the three different electrodes [22]:

$$Q = CV, \tag{3}$$

where Q, and V are the charge and voltage matrices with dimensions of 3×1, respectively. Elements of these matrices are associated with electrode sequences of 1) top electrode, 2) middle electrode and 3) bottom electrode. Therefore, C is a 3×3 capacitance matrix including all capacitances between these three electrodes. The actuation voltage (V_{Act}) is assigned to the top electrode, the sense connection (V_{Sens}) is assigned to the bottom electrode and the middle electrode is terminated

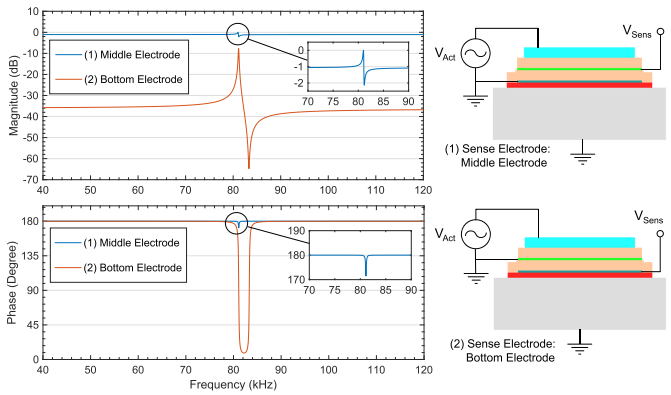

Fig. 3. Simulated magnitude and phase responses of the two-layer cantilever for two different configurations, when middle and bottom electrodes are used as a sense electrode respectively in configuration (1) and (2).

to the ground (GND). Fig. 3 shows magnitudes of the ratio of charges on the sense electrode (Q_{p2}) divided by charges on the actuation electrode (Q_{p1}) i.e. $Q_{\text{Sens}}/Q_{\text{Act}}$ in dB. Note that a voltage of 1 V is assigned to the input voltage, and C_{p1} and C_{p2} are assumed to be identical. Therefore, the charge division represents the voltage division of $V_{\text{Sens}}/V_{\text{Act}}$.

The simulation results compare frequency responses corresponding to two different electrode configurations. The results in blue lines belong to a configuration in which the cantilever is excited by applying a voltage to the top electrode, and the middle electrode is taken as the output. This configuration resembles a cantilever with a single transducer similar to Fig. 1(a). As the simulation results suggest, the cantilever exhibits its first fundamental mode at ~82 kHz. A poor dynamic range is observed in magnitude of the frequency response for this configuration, due to dominance of the feedthrough charge. Similarly, the phase response suggests a poor phase change at resonance, less than 10 degrees. In contrast, in configuration 2, the bottom electrode is used as the readout, while the cantilever is still actuated by the top electrode. The result in orange line shows the frequency response of the cantilever in the second configuration, where a high dynamic range of ~30 dB is noticeable. A change of 180 degree is observable at the resonance. However, presence of an anti-resonance at higher frequency implies the existence of a feedthrough path. To confirm this observation, the capacitance matrix (see Eq. 3) is extracted from the simulation results:

$$C = \begin{pmatrix} 2.32 & -2.27 & -0.03 \\ -2.27 & 4.28 & -2.01 \\ -0.03 & -2.01 & 2.04 \end{pmatrix} pF.$$

The diagonal components of the matrix are the capacitances of each electrode to the ground, while other elements are capacitances between different electrodes. The C_{13} which is the capacitance between the top and the bottom electrodes is 30 fF and more than 70 times smaller than C_{12} and C_{23} capacitances for top and bottom transducers. Therefore, by minimizing the stray feedthrough capacitance C_{ft} (C_{13} in this cantilever) the dynamics of the cantilever becomes dominant to the electrical feedthrough.

III. Fabrication Process

A fabrication process, comprised of seven photomasks, is developed to realize the proposed probes. The process starts with growth of a 500 nm thick thermal oxide layer on an SOI substrate with a highly doped p-type 5 μm thick Si device layer (Fig. 4(a)). The SiO_2 layer isolates the substrate from the bottom electrode. The process continues with a lift-off process of a 200 nm thick Pt bottom electrode (deposited with e-beam evaporation) using the first photo-lithography mask (Fig. 4(b)). In the next step, a stack of three layers of AlN/Mo/AlN with thicknesses of 1 μm/200 nm/1 μm is consecutively deposited. These layers function as the top piezoelectric transducer, the middle electrode and the bottom piezoelectric transducer respectively (Fig. 4(c)). The topmost AlN layer is, then, patterned with the 2$^{\text{nd}}$ mask and etched with a combination of a reactive ion etching (RIE) and a short wet etch process (Fig. 4(d)). For the RIE process a Cl-based plasma is used, where the complementary wet etch is done with a %2.5 tetramethylammonium hydroxide (TMAH) solution to ensure complete removal of the AlN layer. In the next step, the third mask is used to pattern and etch the middle Mo electrode with the Cl-based RIE process (Fig. 4(e)). Then, the 4$^{\text{th}}$ mask is utilized to provide access to the bottom electrodes and pattern the bottom piezoelectric layer (Fig. 4(f)). The bottom piezoelectric layer is also etched with a combination of RIE and wet etch processes similar to step (d). A 500 nm PECVD oxide is, then, deposited which acts as an electrical spacer between the top electrode and two other middle and bottom electrodes. The remainder of the layer is removed from top of the transducers and vias, carved into the oxide layer, to provide electrical connections to the middle and the bottom electrode (Fig. 4(g)). Subsequently, a 1 μm Al top electrode, deposited with a sputtering tool, is lifted-off using the 5$^{\text{th}}$ photo-lithography mask (Fig. 4(h)). With the 6$^{\text{th}}$ mask, the cantilever structure is defined through a lithography step and etched using a deep reactive ion etching (DRIE) process (Fig. 4(i)). At this step, the SOI wafer is flipped over to etch the handle layer underneath the cantilevers using a DRIE process from the backside. Then the cantilevers are fully released by removing the 1 μm thick buried oxide layer from the back with a F-based plasma etch process (Fig. 4(j)). The scanning electron microscope (SEM) image of Fig. 5(a) illustrates the two-layer cantilever.

In the last step, an FEI Nova 200 focused ion beam (FIB) is used to deposit a sharp Pt tip at the free end of the cantilever, together with a pyramid shaped supporting structure (Fig. 5(b)). Such sharp AFM tips have been successfully fabricated and utilized for scanning probe microscopy purposes with microcantilevers in previous works [9], [18]. The tip and its pyramid supporting structure is 7 μm long, and the tip radius is less than 50 nm.

IV. Electromechanical Characterization

Initially, the dynamic response of the microfabricated cantilever is analyzed with a Laser Doppler Vibrometer (LDV), a Polytec MSA-100-3D Micro System Analyzer. The microcantilever is actuated by a periodic chirp signal with an

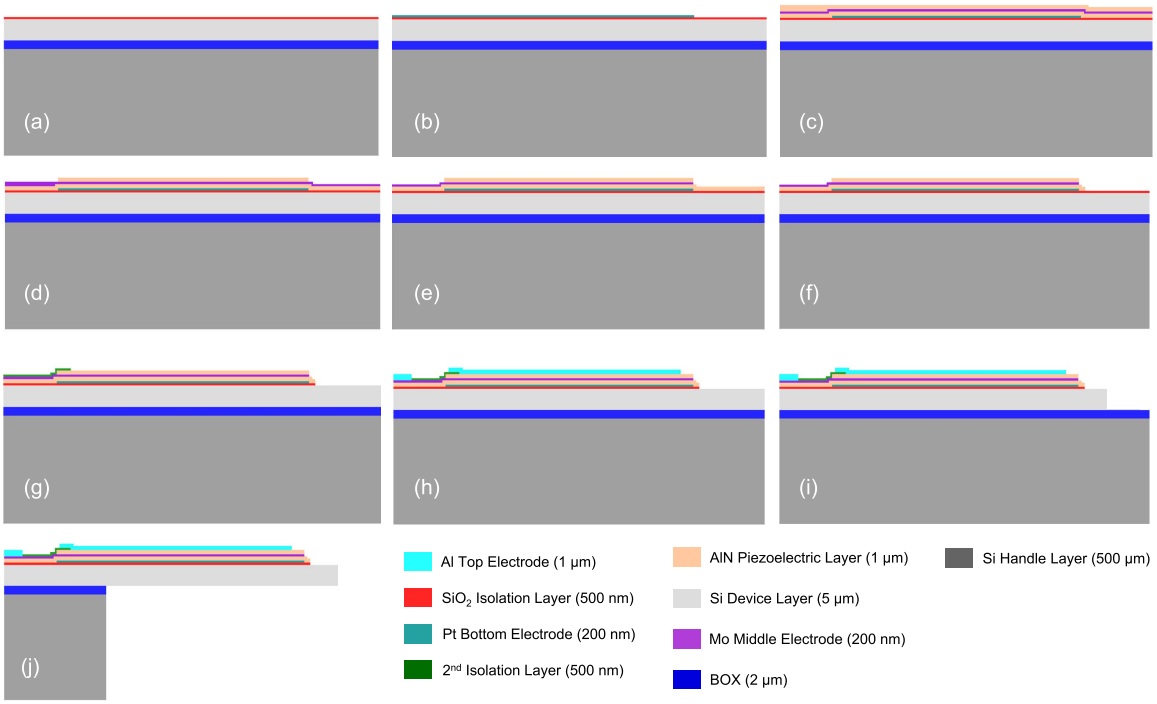

Fig. 4. Microfabrication process flow for realization of two-layer piezoelectric cantilevers: (a) thermal oxide growth, (b) Pt bottom electrode lift-off, (c) double stacked layer depositions, (d) top piezoelectric layer etch, (e) middle Mo electrode etch, (f) bottom piezoelectric layer etch, (g) deposition and formation of oxide spacer, (h) top Al electrode lift-off, (i) device layer etch, and (j) handle and BOX layers etch to release the cantilever.

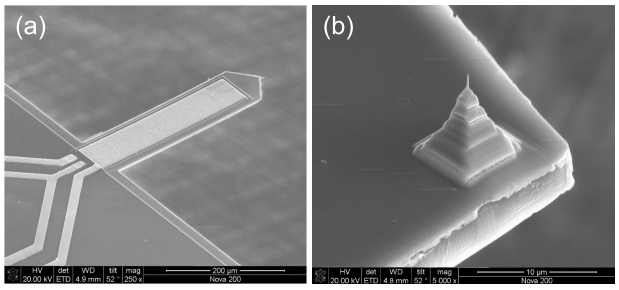

Fig. 5. SEM images of: (a) the fabricated two-layer piezoelectric cantilever, (b) a sharp Pt tip deposited with Focused Ion Beam.

amplitude of 100 mV applied to the top electrode while the middle electrode is grounded. The magnitude and phase frequency responses of the cantilever deflection over a frequency range of 82 kHz to 98 kHz containing the first flexural mode of ∼90 kHz are shown with a dashed green line in Fig. 6.

For electrical characterization of the device, an HF2LI Zurich Instrument lock-in-amplifier (LIA) is used. Similar to the LDV characterization, an AC voltage with an amplitude of 100 mV is applied to the top electrode of the transducer. The middle electrode is connected to the ground, and the bottom (sense) electrode fed to a readout circuit. In the circuit, the output of the piezoelectric cantilever is buffered initially, and is fed to an amplifier circuit with a nominal voltage gain of 100 V/V. The solid red line spectrum in Fig. 6 shows the amplitude of the frequency response of the output voltage divided by the reference voltage from 82 kHz to 98 kHz. It is clear that the piezoelectric deflection sensor magnitude and phase responses completely follow the dynamic response of the cantilever.

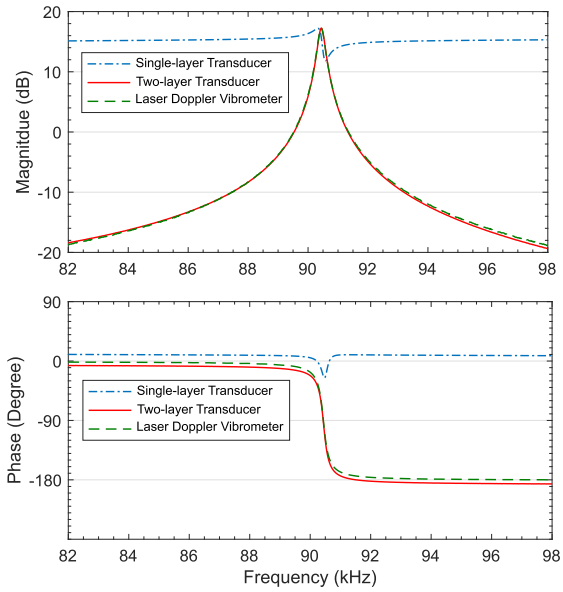

Fig. 6. Displacement frequency responses of the cantilever measured with an LDV (dashed green line), a single piezoelectric transducer (dashed-dotted blue line) and a two-layer transducer (red solid line).

For comparison, the frequency response of the single piezoelectric deflection sensor is acquired. Here, the middle electrode is used as a readout. In contrast with the first configuration, we observe a poor dynamic range and phase response.

Next, wideband frequency responses of the cantilever are obtained with both LDV and piezoelectric sensing methods and plotted in Fig. 7. Three resonance responses

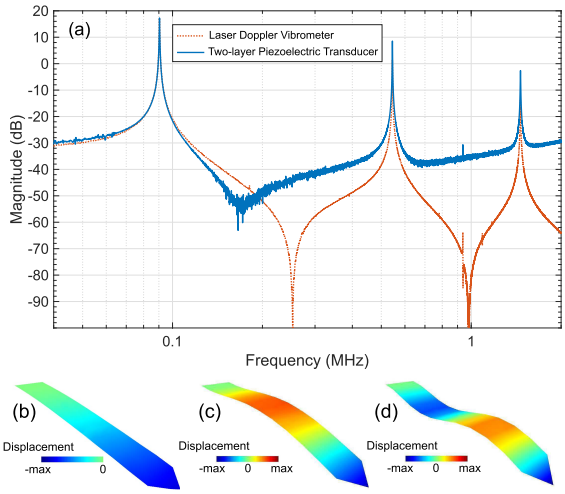

Fig. 7. (a) Wideband frequency spectrum of the cantilever displacement measured with the LDV (dotted orange line) and the piezoelectric sensor (solid blue line). Mode shapes of the dominant resonance modes of the cantilever acquired with LDV: (b) the 1st, (c) the 2nd, and (d) the 3rd modes.

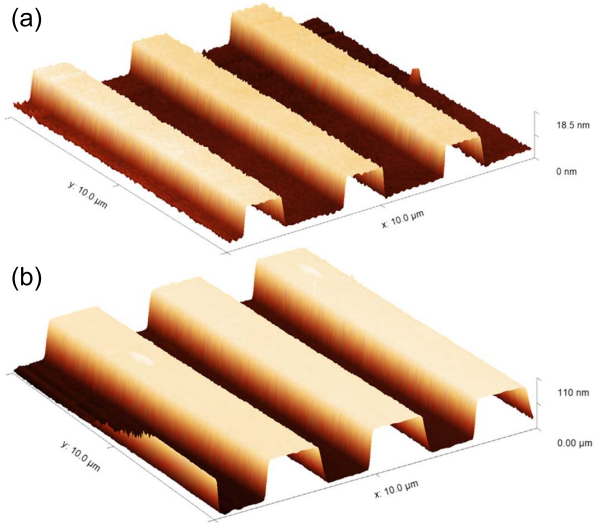

Fig. 8. Results of AFM imaging with the reported cantilever on calibration gratings with steps of: (a) 20 nm and (b) 110 nm features.

are associated with the first mode at ∼90 kHz, the second mode at ∼544 kHz and the third mode at ∼1.462 MHz. Their respective mode shapes are also acquired by LDV and shown in Fig. 7(b), (c) and (d) respectively. It is further evident that, after minimizing the feedthrough, the output response of the tranducer pair follows the collocated displacement response of the cantilever at the tip.

The cantilever is designed to function at the first mode. However, the wideband frequency responses clearly suggest that the effect of the feedthrough has been minimized at higher frequency modes as well. Dynamic ranges as high as ∼40 dB and ∼30 dB are observable at the 2nd and 3rd modes, respectively. Since the modes are widely spaced, the cantilever is an ideal candidate for multifrequency atomic force microscopy [23]. At higher frequencies, the transducer has visibly a high pass characteristics. It should be noted that, although the approach substantially reduces the feedthrough, there exists a small parasitic capactive component between the input and output ports. The capacitive feedthrough impedance decreases at higher frequencies, slightly increasing the crosstalk between the input and the output voltage.

V. AFM Imaging

A. Experimental Setup

The characterized cantilever is used as an AFM probe for tapping mode imaging, operating at its first fundamental resonance frequency. A commercially available AFM (AFM-Workshop TT-AFM) is used to perform raster scanning. For this purpose, the characterized cantilever, and a PCB containing the readout and driving circuits are mounted on a modified cantilever holder, The holder assembly is then inserted into the AFM setup. More details about the setup can be found in [9]. As the cantilever already features on-chip actuation and sensing capabilities, the laser/photo-diode, and the base shaker inside the AFM are bypassed on the breakout interface board. Instead, the actuation signal is provided from the LIA oscillator, and the displacement signal obtained from the the output of the readout circuit is fed into the electronics box of the AFM. The output of the readout circuit is also connected to the LIA for continuous monitoring of the output amplitude. Other essential functions of the AFM for rastering and imaging, including XYZ scanner, PI controller, demodulator, other electronics as well as the associated software are used without any modifications.

B. Imaging

The cantilever is used to obtain the topographic images of two calibration gratings, namely NT-MDT TGZ 20 and TGZ 110, with the sample heights of 20 ± 2 nm and 110 ± 2 nm, respectively. Both gratings feature repeating rectangular steps with a period of 3.00 ± 0.05 μm. Prior to the imaging, the piezoelectric actuator is excited by a 0.1 V signal, to reach the displacement amplitude of 400 nm, validated earlier by the Laser Doppler Vibrometer (LDV). Using the automated approach feature of the commercial AFM, the cantilever is brought into intermittent contact with the surface in order to reach the set amplitude of 300 nm. The cantilever is then raster scanned over the calibration gratings with the scan rate, and scan area set to 0.5 Hz and $10 \times 10\,\mu m^2$ respectively. The obtained 2D and 3D images of the calibration gratings are shown in Fig. 8. The topographic images of both gratings are post-processed by Gywddion using standard built-in tools, such as mean plane subtraction, row alignment, and polynomial background removal [4].

A zoomed FFT spectral analysis of the output voltage of the readout circuit is, also, acquired with the LIA, centered around the first resonance mode (Fig. 9). The red line points at an RMS noise value of −110 dB indicating an SNR of ∼110 dB within a bandwidth of 1 kHz. Based on such SNR, the piezoelectric deflection sensor exhibits a displacement noise density of $600\,fm/\sqrt{Hz}$. Such deflection noise density is comparable to commercial OBD sensors with nominal noise densities in a range of $100 - 1000\,fm/\sqrt{Hz}$ [2].

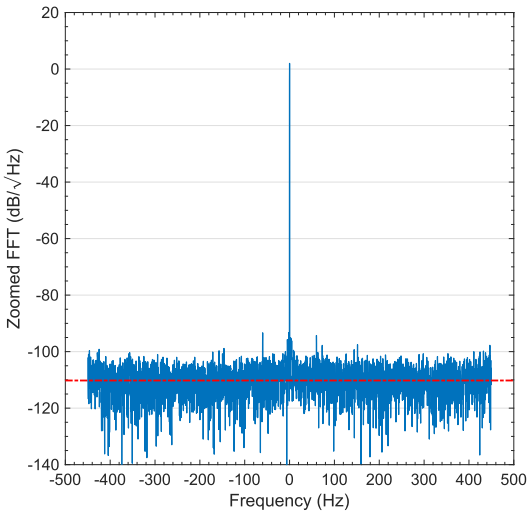

Fig. 9. Zoomed FFT of the output voltage of the cantilever, centered at the first fundamental resonance frequency.

TABLE I
PERFORMANCE COMPARISON OF ACTIVE MICROCANTILEVERS

Reference	Type II [9], [16]	Type I [9], [24]	[19]	TT-2 AFM	[25]	This Work
f_0(kHz)	49.7	49.1	36.4	178.5	57.3	91
Q	397.2	334	369.8	-	20	362
DR [dB]	34.71	27	35	-	17	35.67
SNR [dB]	92	74.1	110.75	119	-	109.3

C. Performance Comparison

The performance of the state-of-the-art active-cantilevers is compared with the proposed piezoelectric cantilever in Table I. The Q-factor, the feedthrough level and the cancellation method are factors which determine the dynamic range of a piezoelectric cantilevers. Therefore, piezoelectric cantilevers reported in [9], [16], [19], [24] with similar Qs are fairly comparable with respect to efficiency of the cancellation method in comparison with the current work. In conclusion, the current work and [19] with minimal inherent feedthrough levels show the highest DRs compared with other methods. On the other hand, signal-to-noise-ratio (SNR) is determined by the noise floor of the readout circuit and amplitude of the output voltage. Higher SNRs are observed for the current work and [19], which show closer SNRs to that of the TT-2 AFM (AFMWorkshop) with an optical lever. The readout circuit can be optimized for achieving higher SNRs. Although similar specs have been attained for the cantilever in [19], the method proposed here is far more suitable for cantilevers with smaller dimensions, and thus faster dynamics, on which placing multi-transducers is not a feasible solution.

VI. CONCLUSION

A new type of piezoelectric microcantilever featuring a very high dynamic range is developed, and used for tapping mode atomic force microscopy. A two-layer piezoelectric stack transducer is microfabricated on the device. One layer serves as an actuator, the other as a sensor. This configuration addresses a major bottleneck associated with piezoelectric cantilevers, i.e. the high feedthrough level from input actuation to readout signal. Eliminating the feedthrough effect, the piezoelectric displacement sensor completely follows the dynamics of the cantilever. This, in turn, enables a high dynamic range and higher signal to noise ratio for achieving a high resolution imaging. This approach enables the designer to maximize the area allocated to sensing, and thus increasing the signal to noise ratio. Future efforts will involve improving the readout circuitry to further enhance the signal to noise ratio and using the cantilever's collocated actuator-sensor pair for Q control. Capturing thermal noise spectrum around the resonance, needed for high resolution dynamic AFM imaging [2], [26]–[30], will be investigated and subsequently reported. Improvement of the readout circuit to function at a lower baseline noise level and enable capturing thermal noise spectrum is part of our ongoing research, which will be reported in future works.

ACKNOWLEDGEMENT AND DISCLAIMER

A. Acknowledgment

This material is based upon work supported by the U.S. Department of Energy's Office of Energy Efficiency and Renewable Energy (EERE) under the Advanced Manufacturing Office Award Number DE-EE0008322.

B. Disclaimer

This report was prepared as an account of work sponsored by an agency of the United States Government. Neither the United States Government nor any agency thereof, nor any of their employees, makes any warranty, express or implied, or assumes any legal liability or responsibility for the accuracy, completeness, or usefulness of any information, apparatus, product, or process disclosed, or represents that its use would not infringe privately owned rights. Reference herein to any specific commercial product, process, or service by trade name, trademark, manufacturer, or otherwise does not necessarily constitute or imply its endorsement, recommendation, or favoring by the United States Government or any agency thereof. The views and opinions of authors expressed herein do not necessarily state or reflect those of the United States Government or any agency thereof.

REFERENCES

[1] R. García, R. Magerle, and R. Perez, "Nanoscale compositional mapping with gentle forces," *Nature Mater.*, vol. 6, no. 6, pp. 405–411, Jun. 2007, doi: 10.1038/nmat1925.

[2] T. Fukuma, M. Kimura, K. Kobayashi, K. Matsushige, and H. Yamada, "Development of low noise cantilever deflection sensor for multienvironment frequency-modulation atomic force microscopy," *Rev. Sci. Instrum.*, vol. 76, no. 5, May 2005, Art. no. 053704, doi: 10.1063/1.1896938.

[3] M. G. Ruppert and S. O. R. Moheimani, "A novel self-sensing technique for tapping-mode atomic force microscopy," *Rev. Sci. Instrum.*, vol. 84, no. 12, Dec. 2013, Art. no. 125006, doi: 10.1063/1.4841855.

[4] M. Dukic, J. D. Adams, and G. E. Fantner, "Piezoresistive AFM cantilevers surpassing standard optical beam deflection in low noise topography imaging," *Sci. Rep.*, vol. 5, Nov. 2015, Art. no. 16393.

[5] J. Adams, L. Manning, B. Rogers, M. Jones, and S. Minne, "Self-sensing tapping mode atomic force microscopy," *Sens. Actuat. A, Phys.*, vol. 121, no. 1, pp. 262–266, May 2005. [Online]. Available: http://www.sciencedirect.com/science/article/pii/S0924424705000130

[6] A. Ahmad *et al.*, "Large area fast-AFM scanning with active 'quattro' cantilever arrays," *J. Vac. Sci. Technol. B, Nanotechnol. Microelectron., Mater., Process., Meas., Phenomena*, vol. 34, no. 6, Nov. 2016, Art. no. 06KM03, doi: 10.1116/1.4967159.

[7] T. Itoh, C. Lee, and T. Suga, "Deflection detection and feedback actuation using a self-excited piezoelectric Pb(Zr,Ti)O_3 microcantilever for dynamic scanning force microscopy," *Appl. Phys. Lett.*, vol. 69, no. 14, pp. 2036–2038, Sep. 1996, doi: 10.1063/1.116871.

[8] B. Rogers, L. Manning, T. Sulchek, and J. Adams, "Improving tapping mode atomic force microscopy with piezoelectric cantilevers," *Ultramicroscopy*, vol. 100, nos. 3–4, pp. 267–276, Aug. 2004. [Online]. Available: http://www.sciencedirect.com/science/article/pii/S0304399104000397

[9] M. B. Coskun, A. G. Fowler, M. Maroufi, and S. O. R. Moheimani, "On-chip feedthrough cancellation methods for microfabricated AFM cantilevers with integrated piezoelectric transducers," *J. Microelectromech. Syst.*, vol. 26, no. 6, pp. 1287–1297, Dec. 2017.

[10] J.-Y. Lee and A. Seshia, "Parasitic feedthrough cancellation techniques for enhanced electrical characterization of electrostatic microresonators," *Sens. Actuators A, Phys.*, vol. 156, no. 1, pp. 36–42, Nov. 2009. [Online]. Available: http://www.sciencedirect.com/science/article/pii/S0924424709000405

[11] Y. Xu and J. E.-Y. Lee, "Single-device and on-chip feedthrough cancellation for hybrid MEMS resonators," *IEEE Trans. Ind. Electron.*, vol. 59, no. 12, pp. 4930–4937, Dec. 2012.

[12] H.-W. Park, Y.-K. Kim, H.-G. Jeong, J. W. Song, and J.-M. Kim, "Feed-through capacitance reduction for a micro-resonator with push–pull configuration based on electrical characteristic analysis of resonator with direct drive," *Sens. Actuators A, Phys.*, vol. 170, nos. 1–2, pp. 131–138, Nov. 2011. [Online]. Available: http://www.sciencedirect.com/science/article/pii/S0924424711003712

[13] H. C. Qiu, P. Schwarz, H. Völlm, D. Feili, X. Z. Wu, and H. Seidel, "Electrical crosstalk in two-port piezoelectric resonators and compensation solutions," *J. Micromech. Microeng.*, vol. 23, no. 4, Apr. 2013, Art. no. 045007, doi: 10.1088/0960-1317/23/4/045007.

[14] M. Kangul, E. Aydin, F. Gokce, O. Zorlu, and H. Kulah, "Analysis and elimination of the capacitive feedthrough current on electrostatically actuated and sensed resonance-based MEMS sensors," *J. Microelectromech. Syst.*, vol. 26, no. 6, pp. 1272–1278, Dec. 2017.

[15] J. Arcamone, E. Colinet, A. Niel, and E. Ollier, "Efficient capacitive transduction of high-frequency micromechanical resonators by intrinsic cancellation of parasitic feedthrough capacitances," *Appl. Phys. Lett.*, vol. 97, no. 4, Jul. 2010, Art. no. 043505, doi: 10.1063/1.3472217.

[16] M. B. Coskun, H. Alemansour, A. G. Fowler, M. Maroufi, and S. O. R. Moheimani, "Q control of an active AFM cantilever with differential sensing configuration," *IEEE Trans. Control Syst. Technol.*, vol. 27, no. 5, pp. 2271–2278, Sep. 2019.

[17] M. G. Ruppert and S. O. R. Moheimani, "Multimode Q control in tapping-mode AFM: Enabling imaging on higher flexural eigenmodes," *IEEE Trans. Control Syst. Technol.*, vol. 24, no. 4, pp. 1149–1159, Jul. 2016.

[18] M. G. Ruppert, A. G. Fowler, M. Maroufi, and S. O. R. Moheimani, "On-chip dynamic mode atomic force microscopy: A silicon-on-insulator MEMS approach," *J. Microelectromech. Syst.*, vol. 26, no. 1, pp. 215–225, Feb. 2017.

[19] M. G. Ruppert, S. I. Moore, M. Zawierta, A. J. Fleming, G. Putrino, and Y. K. Yong, "Multimodal atomic force microscopy with optimized higher eigenmode sensitivity using on-chip piezoelectric actuation and sensing," *Nanotechnology*, vol. 30, no. 8, Feb. 2019, Art. no. 085503, doi: 10.1088/1361-6528/aae40b.

[20] A. Schuh, I. S. Bozchalooi, I. W. Rangelow, and K. Youcef-Toumi, "Multi-eigenmode control for high material contrast in bimodal and higher harmonic atomic force microscopy," *Nanotechnology*, vol. 26, no. 23, Jun. 2015, Art. no. 235706, doi: 10.1088/0957-4484/26/23/235706.

[21] S. O. R. Moheimani and A. J. Fleming, *Piezoelectric Transducers for Vibration Control and Damping*. London, U.K.: Springer-Verlag, 2006.

[22] A. Ruehli and P. Brennan, "Capacitance models for integrated circuit metallization wires," *IEEE J. Solid-State Circuits*, vol. 10, no. 6, pp. 530–536, Dec. 1975.

[23] S. Sadewasser, G. Villanueva, and J. A. Plaza, "Special cantilever geometry for the access of higher oscillation modes in atomic force microscopy," *Appl. Phys. Lett.*, vol. 89, no. 3, Jul. 2006, Art. no. 033106, doi: 10.1063/1.2226993.

[24] A. G. Fowler, M. B. Coskun, and S. O. R. Moheimani, "Q control of a microfabricated piezoelectric cantilever with on-chip feedthrough cancellation," in *Proc. IEEE Conf. Control Technol. Appl. (CCTA)*, Aug. 2017, pp. 123–128.

[25] G. E. Fantner, D. J. Burns, A. M. Belcher, I. W. Rangelow, and K. Youcef-Toumi, "DMCMN: In depth characterization and control of AFM cantilevers with integrated sensing and actuation," *J. Dyn. Syst., Meas., Control*, vol. 131, no. 6, 2009, Art. no. 061104. [Online]. Available: https://doi.org/10.1115/1.4000378

[26] A. P. Nievergelt, J. D. Adams, P. D. Odermatt, and G. E. Fantner, "High-frequency multimodal atomic force microscopy," *Beilstein J. Nanotechnol.*, vol. 5, pp. 2459–2467, Dec. 2014.

[27] F. J. Giessibl and B. M. Trafas, "Piezoresistive cantilevers utilized for scanning tunneling and scanning force microscope in ultrahigh vacuum," *Rev. Sci. Instrum.*, vol. 65, no. 6, pp. 1923–1929, Jun. 1994, doi: 10.1063/1.1145232.

[28] J. L. Arlett, J. R. Maloney, B. Gudlewski, M. Muluneh, and M. L. Roukes, "Self-sensing micro-and nanocantilevers with attonewton-scale force resolution," *Nano Lett.*, vol. 6, no. 5, pp. 1000–1006, May 2006, doi: 10.1021/nl060275y.

[29] T. Fukuma, "Wideband low-noise optical beam deflection sensor with photothermal excitation for liquid-environment atomic force microscopy," *Rev. Sci. Instrum.*, vol. 80, no. 2, Feb. 2009, Art. no. 023707, doi: 10.1063/1.3086418.

[30] F. J. Giessibl, "The qPlus sensor, a powerful core for the atomic force microscope," *Rev. Sci. Instrum.*, vol. 90, no. 1, Jan. 2019, Art. no. 011101, doi: 10.1063/1.5052264.

Mohammad Mahdavi received the B.Sc. and M.Sc. degrees in electrical engineering from The University of Tehran, Tehran, Iran, in 2007 and 2010, respectively, and the Ph.D. degree in electrical engineering from The University of Texas at Dallas in May 2018. He is currently a Research Scientist with the Department of Systems Engineering, The University of Texas at Dallas. His main research interests include design, microfabrication, and characterization of MEMS devices with a special emphasis on resonant piezoelectric devices and high-speed scanning probe microscopy.

M. Bulut Coskun received the B.Sc. and M.Sc. degrees in mechatronics engineering from Sabanci University, Istanbul, Turkey, in 2009 and 2011, respectively, and the Ph.D. degree in mechanical and aerospace engineering from Monash University, Australia, in 2015. Later on, he joined the Department of Mechanical Engineering, The University of Texas at Dallas, as a Research Associate, where he developed active cantilevers, cantilever arrays, and nanopositioners for high-speed and high-throughput scanning probe microscopy applications. In late 2019, he joined the Jet Propulsion Laboratory. His current research interests include design, analysis, fabrication, and characterization of micro/nanoelectromechanical systems with a particular emphasis on surface acoustic wave devices.

S. O. Reza Moheimani (Fellow, IEEE) currently the James Von Ehr Distinguished Chair of science and technology with the Department of Systems Engineering, The University of Texas at Dallas with appointments at Electrical and Computer Engineering and Mechanical Engineering Departments. His current research interests include applications of control and estimation in high-precision mechatronic systems, high-speed scanning probe microscopy, and atomically precise manufacturing of solid-state quantum devices. He is a fellow of the IFAC and the Institute of Physics, U.K. He is a recipient of several awards, including the IFAC Nathaniel B. Nichols Medal and the IEEE Control Systems Technology Award. He is the Editor-in-Chief of *Mechatronics*.